Materials and Manufacturing Processes

ISSN: 1042-6914 (Print) 1532-2475 (Online) Journal homepage: www.tandfonline.com/journals/lmmp20

Plasma synthesis of ammonia by asymmetric electrode arrangement

F. Baharlounezhad, M.A. Mohammadi & M.S. Zakerhamidi

To cite this article: F. Baharlounezhad, M.A. Mohammadi & M.S. Zakerhamidi (2023) Plasma synthesis of ammonia by asymmetric electrode arrangement, Materials and Manufacturing Processes, 38:2, 159-169, DOI: 10.1080/10426914.2022.2105875

To link to this article: https://doi.org/10.1080/10426914.2022.2105875

Published online: 31 Jul 2022.

MATERIALS AND MANUFACTURING PROCESSES
2023, VOL. 38, NO. 2, 159–169
https://doi.org/10.1080/10426914.2022.2105875

Plasma synthesis of ammonia by asymmetric electrode arrangement

F. Baharlounezhad, M.A. Mohammadi, and M.S. Zakerhamidi

Faculty of Physics, University of Tabriz, Tabriz, Iran

ABSTRACT

The plasma reactors are of great interest in ammonia synthesis because of their green performance, small-scale process capabilities, and various design and application options. The purpose of this research is to synthesize water-soluble ammonia by plasma electrolysis which utilizes nitrogen atmospheric pressure plasma generated by DC discharge. Then, we investigate the influence of the plasma characteristics such as the electron temperature and density on the resultant ammonia concentration. For this purpose, the model of the Hoffman electrolysis apparatus was designed for separating the anodic and the cathodic parts, producing plasma, and finally interacting with an aqueous solution surface. This procedure allows us to compare the mechanism of the classical electrolysis with plasma electrolysis. The concentration of synthesized ammonia resulting from the reaction of active species in the interaction between plasma and the liquid surface on the cathode side of the device was obtained. The plasma electron temperature and density were measured by the standard Boltzmann plot method and the Stark broadening of $H_\beta$via optical emission spectroscopy (OES), respectively, and their effects on the interaction between plasma and the water surface were investigated, which leads to nitrite and ammonia synthesis. The intensity of the emitted light varied as the discharge voltage was increased according to 8kV, 9kV, 10kV, and 11kV. As a result, the plasma electron temperature, density, and the synthesis of additional water-soluble ammonia parameters increase. Multiple parameter linear regression was used to evaluate the effect of varying the voltage on these parameters, which was positive.

ARTICLE HISTORY
Received 29 March 2022
Accepted 23 June 2022

KEYWORDS
Plasma; electrolysis; ammonia; temperature; density

Introduction

Plasma as the fourth state of matter is produced by the ionization of neutral gases, resulting in an equal number of positive ions and negative electrons in two forms: thermal plasma (TP) and non-thermal plasma (NTP). Thermodynamic equilibrium characterizes thermal plasma, which means that all species have the same temperature. Non-thermal plasma is not in thermal equilibrium where electrons, due to their small mass, are usually at the temperature of about$T_e = 1eV$, and the temperature of the background gas molecules (T_0) is close to room temperature$(T_e \gg T_0)$. NTP contains extremely reactive electrons, ions, atoms, and radicals, allowing it to be employed in the production of a variety of materials such as diamonds,[1–3] metal nano-particles,[4–6] ceramic nano-powders,[7,8] nano-fibers,[9,10] nano-crystals,[11,12] ozone,[13–15] and ammonia.[16,17] By nitrogen fixation and a significant increase in chemical kinetics, NTP can enable ammonia production at room temperature and atmospheric pressure. Glow discharges,[18–20] microwaves (MW),[21,22] radio frequencies (RF),[21,23] and dielectric barrier discharge (DBD) plasma reactors [24–26] have all been used to synthesize ammonia. The RF and MW discharges are expensive methods due to vacuum equipment. Also, DBD has uncontrollable conditions caused by AC current.

In the chemical industry, ammonia is one of the most extensively used materials.[27,28] In addition, it is an important nitrogen compound in fertilizers preparation,[29] a reducing agent in nitrogenization processes,[30] a source of energy supply, and a low-cost fuel compared to other fuels.[31] Ammonia can be synthesized in many ways, including thermochemical synthesis (Haber-Bosch process),[32,33] electrochemical synthesis,[34,35] dense metal membranes,[36] the oxidation-reduction cycle of solar thermochemical,[37–39] and non-thermal plasma.[40,41] Chemical and plasma physics engineers have been interested in using the non-thermal plasma approach for the synthesis of ammonia from the mixture (N_2 and H_2 gas) through NH_x radicals as a clean and small-scale alternative in recent decades.

Electrolysis is the process of passing an electric current through the material to cause a chemical change. This process takes place in an electrolytic cell, a reactor consisting of cathode and anode electrodes immersed in a solution containing positive and negative charged ions. An electrolytic cell, also known as an electrolysis reactor, converts electrical energy into chemical energy. Metal conductors are used as electrodes in electrolysis reactors. Electrodes are responsible for the transmission of electrons in certain circumstances and are also engaged in electrolysis processes in others. The cathode is the electrode that sends electrons to the anode across the electrolyte environment, and the anode is the electrode that receives electrons from the cathode. Electrolysis is widely used in metallurgical engineering [42,43] like electrowinning,[44,45] electrorefining,[46–48] and electroplating.[49,50] The electrodes of an electrochemical system with asymmetric electrode configurations might differ in form, size, material, and design from one another.

CONTACT M. A. Mohammadi mohammadidorbash@yahoo.com; m_a_mohammadi@tabrizu.ac.ir Faculty of Physics, University of Tabriz, Tabriz, Iran

It may be noted that the use of plasma electrolysis and atmospheric discharge has been continuously investigated in the recent past on ammonia synthesis. However, the effect of plasma parameters on ammonia synthesis has been less explored as per literature. In this study, ammonia has been synthesized with NTP in an asymmetric electrode configuration resulting from a glow discharge at various electron temperatures and densities by varying the discharge voltage. The experimental current of this study was in the glow region and glow-to-arc-transition, therefore discharged was considered glow.[51] Plasma electrolysis produces a highly reactive interfacial liquid layer in interaction with liquid due to various processes driven through electrons, ions, photons, and radicals that are produced by the plasma. In this system, electrons are generated in the plasma and transferred to the interfacial liquid or injected into the interface by electric fields. This few tens of nanometers surface layer has been compared to classical electrolysis, in which a solid electrode inserts dissolved electrons directly into the electrolyte solution. While there are many differences between classical electrolysis and plasma electrolysis, plasma–liquid interactions can be considered in the first approximation as the replacement of a metal electrode in an electrolytic cell with plasma.[52] The mechanism and chemical reactions of the electrolysis and plasma electrolysis methods were described and compared. Plasma electron temperature and density were determined at different discharge voltages by the Stark broadening of the hydrogen Balmer H_β spectral line and the Boltzmann plot using the plasma emission spectroscopy of glow discharge, respectively. Finally, the ammonia synthesis findings were compared to discharge voltage changes, and variation plasma electron temperature and density.

Materials and methods

Materials

A pH indicator bromothymol blue (BTB, $C_{27}H_{28}Br_2O_5S$) was used to display pH changes on the anode and the cathode sides of the electrolysis reactor. The aqueous solution of BTB is blue in undefined.60, yellow in undefined.00, and green in undefined.00–7.60. Distilled water (pH = 6.21), sodium chloride (NaCl), and sodium perchlorate ($NaClO_4$) were used to prepare the solutions of the Hoffman reactor. The reactor was filled with distilled water which was washed with nitrogen gas for one hour. Nitrogen gas produced atmospheric pressure plasma of the DC discharge. All the materials in this study were the high extra pure grade from Merck.

Instruments and methods

We used the plasma electrolysis method to manufacture ammonia at room temperature and atmospheric pressure, which includes the interaction of nitrogen plasma with an aqueous solution surface, which is different from plasma-activated water. Plasma activated water is long process completion time, while the applied method has short time changing environmental conditions. In plasma activated water, active species and ions lead to acidic pH in the solution, which is greater in cathode rather than in anode.[53] The experimental setup for this study is shown in Fig. 1. An H-shaped Pyrex glass reactor, the Hoffman electrolysis reactor, was used to separate the anodic and the cathodic reactions. The Hoffman electrolysis reactor allows investigating the influence of electron or negative ion reactions in interface with the aqueous solution surface apart from positive ion reactions. The reactor electrodes were selected from tungsten rods with a diameter of 2 mm. The classical electrolysis was performed with tungsten electrodes immersed in the liquid at 8kV. The cathodic tungsten rod was inserted into a *T*-shaped glass tube, 1.5 mm out of the aqueous solution surface, for gas flow in plasma electrolysis. Despite operating at atmospheric pressure, the cathode side was completely protected by nitrogen gas, ambient air and oxygen gas did not reach the cathode and were not involved in plasma formation. As a result, only the electron temperature of the nitrogen gas plasma was calculated. Aqueous solution pH was measured with WTW Lab-pH Meter inoLab® pH 7110 with a numerical precision of 0.01. Nitrogen gas flowed through a *T*-shaped tube to the liquid surface and was ionized by applying a high potential difference between the electrodes. The mass flow controller was adjusted in 50sccm. The

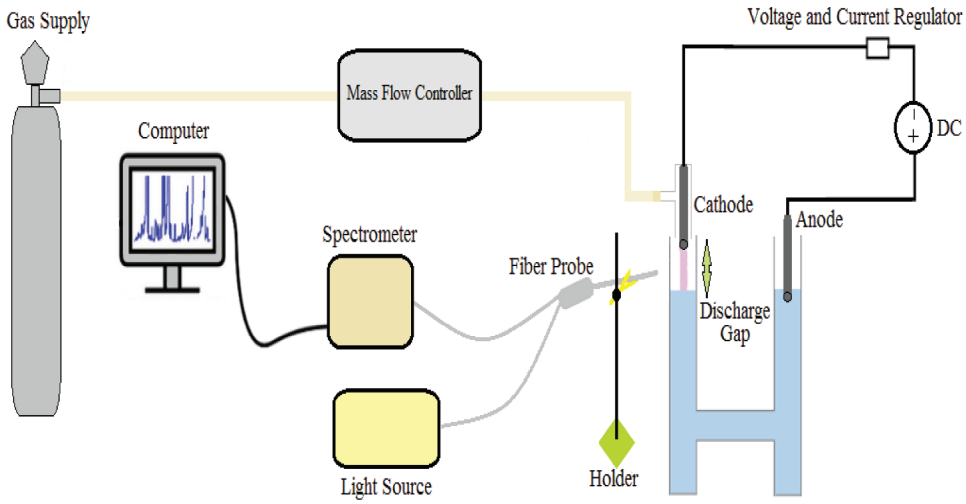

Figure 1. Experimental setup of DC glow discharge reactor.

discharge gap on the cathode side on the surface of the aqueous solution was 1.5 mm. The reactor of DC glow discharge operated at 8kV, 9kV, 10kV, and 11kV.

Emission spectroscopy was performed with a miniature optical spectrometer (UV-Vis-NIR), over the wavelength range of 190–850 nm with a wavelength accuracy of ±0.1 nm, manufactured by Pooyesh Tadbir Karaneh Co. A double beam UV-Vis spectrophotometer (Shimadzu UV-2450), with a measuring wavelength range of 190-900 nm and a wavelength accuracy of ±.01 nm, was used to record the absorbance spectra of (ClO^-) and ammonia. Measurement of ammonia concentration was done by High-Performance Liquid Chromatography (HPLC), D -14163 KNAUER. Nitrite anion was confirmed by ion chromatography (930 Compact IC Flex, 150 mm version of the Metrosep A Supp 5 - 150/4.0) Made by Metrohm company with the particle size of 5 µm.

Result and discussion

Classical electrolysis and plasma electrolysis

The properties of classical electrolysis and plasma electrolysis, as well as their products, were compared first, and then the reactions were determined. Figure 2 shows two tungsten rods immersed in a solution (NaCl, 0.50 M) with a small amount of BTB added. The aqueous solution was treated 10 min under 0.25 mA constant current electrolysis at 8kV.

The electrolyte reaction in sodium chloride solution is defined as follows [54,55]

$$2H_2O(l) + 2e^- \rightarrow H_2(g) + 2OH^-(aq) \text{Half cathodic reaction} \quad (1)$$

$$2Cl^-(aq) \rightarrow Cl_2(g) + 2e^- \text{Half anodic reaction} \quad (2)$$

The reactions indicate the production of $H_2(g)$ on the cathode side and $Cl_2(g)$ on the anode side. There is a superiority of the water molecule in competition with the positive ion of the water-soluble sodium on the cathode side. In contrast, there is a predominance of negative ion of the water-soluble chlorine with the water molecule on the anode side. Initially, the solution pH was 7.3. As shown in Fig. 2, the liquid on the cathode side has changed to blue (pH = 9.00) due to hydroxide ions production (OH^-) that alkalizes the liquid during 10 min. The liquid around the anode is decolorized during the electrolysis. This decolorization is due to the partial dissolution of chlorine gas (Cl_2) in water, hypochlorous acid production (HClO), and overcoming hydrogen ion (H^+),[55] which results in acidification of aqueous solution (pH = 6.82) on the anode side. The equation of the chemical process occurring on the anode electrode side is as follows:

$$H_2O(l) + Cl_2(g) \rightarrow HCl(aq) + HClO(aq) \quad (3)$$

Figure 3 shows plasma electrolysis of solution (NaCl, 0.5 M) containing BTB by nitrogen gas plasma for 10 min after the beginning of electrolysis at a constant current of 0.6 mA. As can be seen, the aqueous solution on the cathode side has changed to blue (alkaline, pH = 10.10), and on the anode side to yellow (acidic, pH = 3.51). Chlorine gas production in plasma electrolysis is less than in classical electrolysis. Therefore, the concentration of production hypochlorous acid is low, which does not lead to the decomposition of BTB. Hypochlorous acid (HClO) has a high oxidative capacity, thus it can breakdown BTB and decolorize the aqueous solution around the anode instead of turning it yellow.[55]

The amount of discoloration depends on the concentration of hypochlorous acid produced during electrolysis. Figure 4a shows the calibration curve of the standard solution ($NaClO_4$) at 0.0010 M, 0.0055 M, 0.0100 M, 0.0550 M, and 0.1000 M concentrations to determine the quantity of $ClO^-$and Fig. 4b represents the absorption spectrum of the aqueous solution containing ClO^- after the classical electrolysis and plasma electrolysis. Obtained results show that the concentration of HClO in the classical electrolysis (1.1270 M) was higher than plasma electrolysis (0.8640 M).

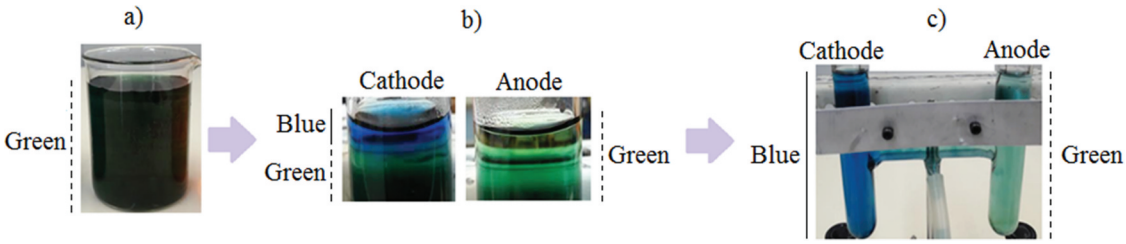

Figure 2. Aqueous solution (NaCl, 0.5 M), a) before, b) after 3 min, and c) after 10 min the classical electrolysis.

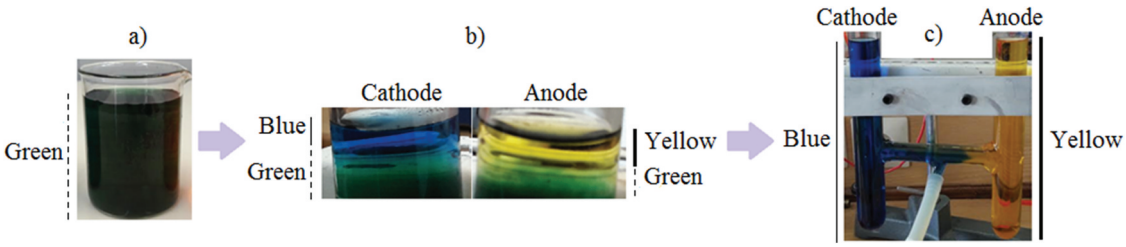

Figure 3. Aqueous solution (NaCl, 0.5 M), a) before, b) after 3 min, and c) after 10 min plasma electrolysis.

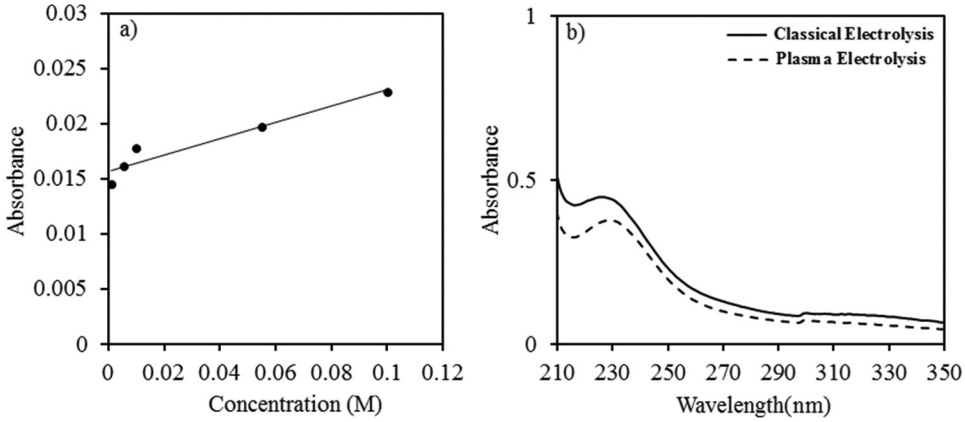

Figure 4. a) The calibration curve of the standard solution($NaClO_4$), b) Adsorption spectra of solution containing ClO^- after the classical electrolysis and plasma electrolysis.

Henceforth, the reactor solution was selected distilled water and the reactions leading to ammonia synthesis were investigated. Water electrolysis is the process of dissociating water molecules into hydrogen and oxygen gases using electrical power. The electrochemical reactions that happened on the cathode side follow as [56]

$$2H^+ + 2e^- \rightarrow H_2(g) \quad (4)$$

$$2H_2O(l) + 2e^- \rightarrow H_2(g) + 2OH^- \quad (5)$$

and the dominant electrochemical reaction on the anode side are [56]

$$2H_2O(l) \rightarrow O_2(g) + 4H^+ + 4e^- \quad (6)$$

$$4OH^- \rightarrow O_2(g) + 2H_2O(l) + 4e^- \quad (7)$$

The reaction in used plasma electrolysis is different from classical electrolysis because in plasma electrolysis, electron irradiation to the solution surface is induced by some reactions such as decomposition, ionization, charge transfer, and evaporation. At the cathode, the surface reaction occurs mostly along the solution–plasma interface, where free electrons are transported from the plasma into the solution, forming a thin layer of solvated electrons.[57] In the plasma electrolysis setup, nitrogen plasma is produced and current conducted via the water. Plasma activation of the water is referred to as plasma-activated electrolyte. Around the cathode, hydrogen gas is produced via plasma generation between the electrode and the water surface.[58] Plasma electron irradiation produces hydroxide ion(OH^-). Non-thermal plasma can activate the water and nitrogen gas, producing reactive nitrogen compounds NO_X dissolved in solution as an intermediary for ammonia's (NH_4^+) electrochemical synthesis. The total concentration of NO_X increases linearly as a function of plasma exposure time. Here, exist of nitrite ion(NO_2^-) confirmed at the cathode electrode side. Nitrite ion is soluble, much more easily reduced to ammonia than N_2 gas. To produce ammonia, a reaction field must be created in which active nitrogen species may react with hydrogen gas. Ammonia could only be made lower potentials than water reduction, where most electrons would approve H_2 gases generations.[59] The given conditions are provided by the cathode side. These cathodic reactions in used plasma electrolysis system are

$$2H_2O(l) + 2e^- \rightarrow H_2(g) + 2OH^- \quad (8)$$

$$2H^+ + 2e^- \rightarrow H_2(g) \quad (9)$$

$$NO_2^-(aq) + 8H^+ + 6e^- \rightarrow NH_4^+(aq) + 2H_2O(l) \quad (10)$$

$$NH_4^+(aq) + OH^- \rightarrow NH_3(aq) + 2H_2O(l) \quad (11)$$

Nitrogen ion from direct ionization by electron impact can react with hydrogen gas. A possible ion-molecule reaction mechanism for the synthesis of ammonia is shown below [60]

$$N^+ + H_2(g) \rightarrow NH^+(aq) + H \quad (12)$$

$$NH^+ + H_2(g) \rightarrow NH_2^+(aq) + H \quad (13)$$

$$NH_2^+ + H_2(g) \rightarrow NH_3^+(aq) + H \quad (14)$$

In this system, nitrogen plasma interacted with the water surface at 8kV, 9kV, 10kV, and 11kV for 20 min. The concentrations of synthesized water-soluble ammonia on the cathode side were reported by UV-Vis spectrophotometer at 5.879×10^{-6}M,1.470×10^{-5}M,1.176×10^{-4}M, and 1.764×10^{-4}M respectively. The results were confirmed by HPLC.

It is reasonable to consider that the acidification of the solution at the anode side is due to the dissolved hydrogen ion (H^+) and nitrite, which flown from the cathode to the anode. In addition, oxygen gas is generated in the vicinity of the anode.[61]

$$2H_2O(l) \rightarrow O_2(g) + 4H^+ + 4e^- \quad (15)$$

$$NO + H_2O \rightarrow NO_2^- + 2H^+ + e^- \quad (16)$$

The concentrations of hydrogen ions (H^+) on the anode side and hydroxide ions (OH^-) on the cathode side were calculated using pH and pOH in both electrolysis, and their changes, Figs. 5 and 6, were described over time, respectively. According to Fig. 5, the maximum concentration of hydrogen

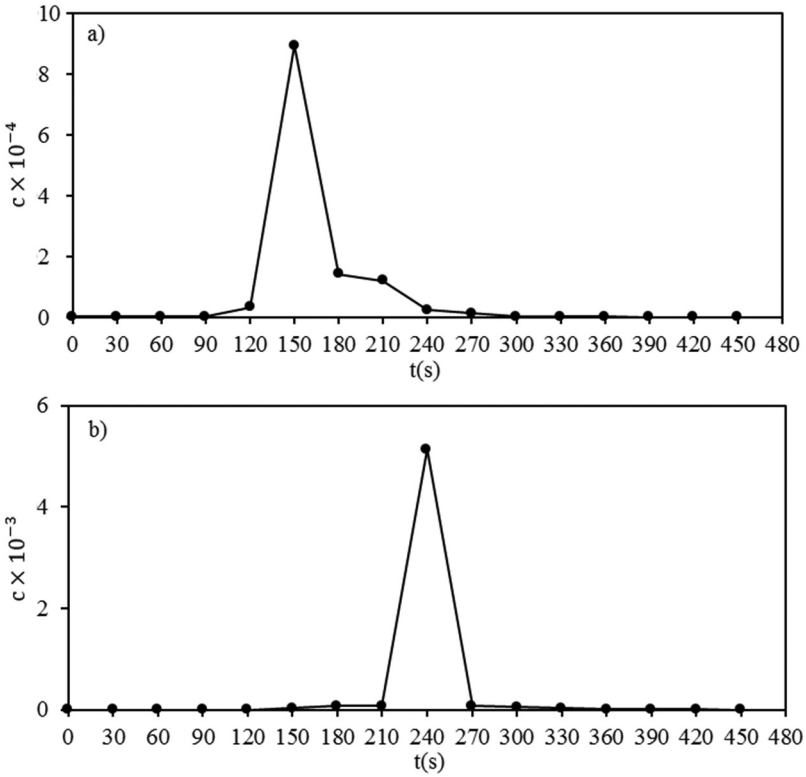

Figure 5. The hydrogen ion concentration changes on the anode side in a) the classical electrolysis and b) plasma electrolysis (The hydrogen ion concentration was calculated through solution pH).

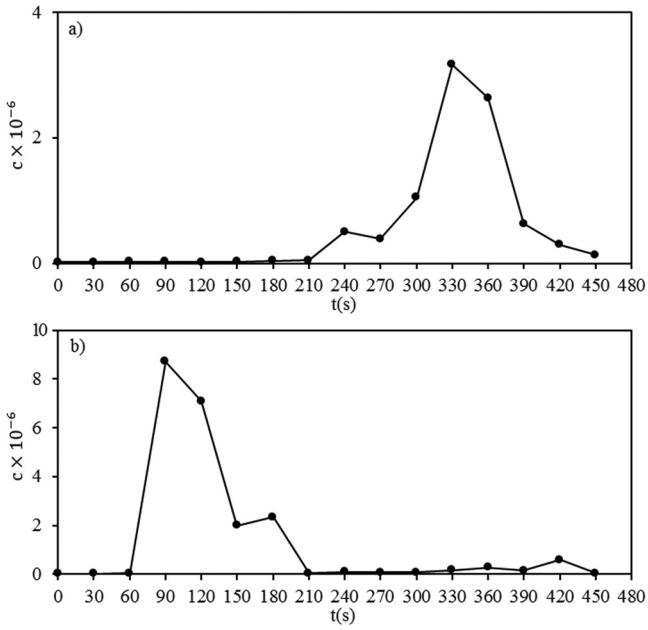

Figure 6. The hydroxide ion concentration changes on the cathode side in a) the classical electrolysis and b) plasma electrolysis.

ions on the anode side in the classical electrolysis was lower than plasma electrolysis. In addition, the concentration of hydrogen ions on the anode side in the classical electrolysis increased over a shorter time than in plasma electrolysis to reach equilibrium. This demonstrates that additional species than hydrogen ions, such as nitrite on the anode side, engage in the reaction with hydrogen ions in plasma electrolysis. It prolongs the reaching equilibrium time. NO_2^- concentration on the anode side was obtained ~0.1 ppm at equilibrium time.

According to Fig. 6, the maximum concentration of hydroxide ions on the cathode side in the classical electrolysis is lower than plasma electrolysis, and it has been elevated for a longer period to attain equilibrium than plasma electrolysis. It shows that in plasma electrolysis, the production of ammonia, and the reaction of the NO_2^- andH^+ leading to NH_4^+ increase the alkaline property and concentration of the hydroxide ion. It shortens the reaching equilibrium time. NO_2^- and ammonia concentrations were obtained ~0.380 ppm and ~0.200 ppm at equilibrium time, respectively.

The pH-dependent anodic and cathodic half-reactions formed during the classical electrolysis and plasma electrolysis are presented by the Pourbaix diagram, (E-pH), in an aqueous solution. The equilibrium potentials of electrochemical processes are shown versus pH in a Pourbaix diagram, which displays probable stable states in an aqueous electrochemical system. The lines that connect the areas on the diagram define the thermodynamic stability zones of the products. According to the water Pourbaix diagram in Fig. 7, reactions in the classical electrolysis on the anode side at potentials above line 1 and on the cathode side at potentials below line 2 in favor of O_2 and H_2 proceed from H_2O, respectively.[62,63]

The nitrogen Pourbaix diagram in the aqueous electrochemical system of plasma electrolysis is shown in Fig. 8. In this case, in addition to the production of O_2 and H_2, the reactions at potentials below line 3 take place to produce NO_2^- on the

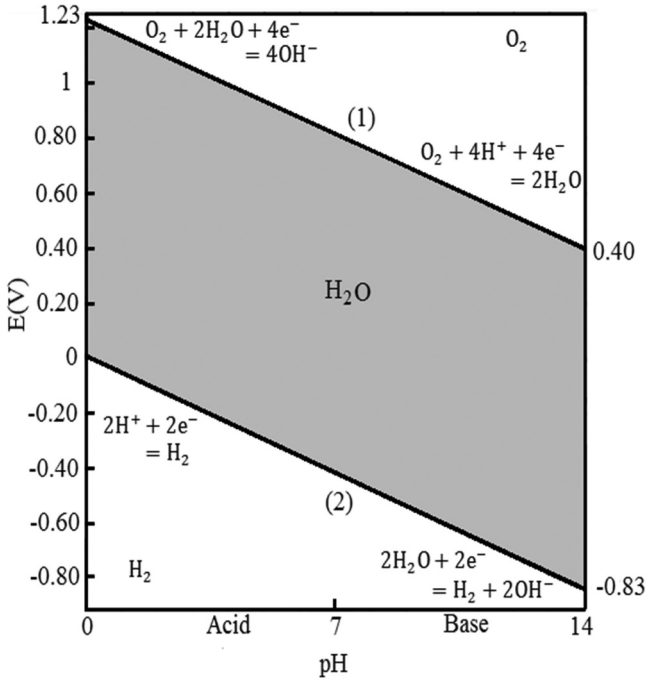

Figure 7. Pourbaix diagram of water in the classical electrolysis.

anode side. The reactions above and below line 4 occur to the production of NO_2^- and NH_3 on the cathode side, respectively.[64–66]

Determination of plasma electron temperature and density

To determine the plasma electron temperature, the discharge spectrum was evaluated for each voltage using the standard Boltzmann plot method. The Boltzmann plot is a frequently used spectral measurement method, particularly for evaluating plasma electron temperature by spectral line emission intensity. In this method, four suitable lines of (N I) were selected from the spectral lines of nitrogen plasma discharge. The used equation for calculation of the plasma electron temperature is defined as follows [67,68]

$$\ln\frac{I_{ji}\lambda_{ji}}{A_{ji}g_j} = -\frac{E_j}{k_B T} + c \tag{17}$$

where I_{ji} is the intensity of the spectral line, $\lambda_{ij}(\text{nm})$ is the wavelength of the emitted light, which is the probability per second that an atom in state j spontaneously emits in a random direction and is de-excited to state i, g_j is the statistical weight of the energy level, $A_{ji}(s^{-1})$ is transition probability, $k_B = 1.38 \times 10^{-23}(\text{J/K})$ is Boltzmann constant, T(eV) is plasma electron temperature, $E_j(\text{eV})$ is energy level of the upper state for emission and c is a constant value. To create the Boltzmann plot, $\ln\left(I_{ji}\lambda_{ji}/A_{ji}g_j\right)$ is plotted against E_j in eV, using Table 1 data.[69,70]

Figure 9 shows Boltzmann plot for calculating electron temperature from nitrogen plasma emission spectroscopy at 8 kV.

The electron temperature in glow discharge nitrogen plasma has been calculated in the wavelength range λ = 439–586 (nm), which according to Fig. 10, values of 0.8702 eV, 0.9210 eV, 0.9594 eV, and 0.9800 eV were obtained at 8kV, 9kV, 10kV, and 11kV, respectively.

The Stark effect describes how spectral lines can be divided or shifted in the presence of external electric fields caused by other particles in the plasma.[71] The Stark effect on hydrogen eliminates the degeneracy of states with the same principal quantum number (n) and the different angular quantum number (l), resulting in the Stark broadening commensurate with the strength of the field. This broadening directly related to electron density in plasma discharge is used to determine plasma density. The Stark broadening of the hydrogen Balmer H_β spectral line was exerted to measure the electron

Table 1. Atomic data of chosen N I lines.

Wavelength (nm)	Statistical Weight	Transition Probability ($10^8 s^{-1}$)	Upper Level Energy (eV)
439.24	2	0.0102	14.9483
536.7	4	0.00118	13.2388
537.26	4	0.00107	13.2364
585.6	2	0.0076	13.9563

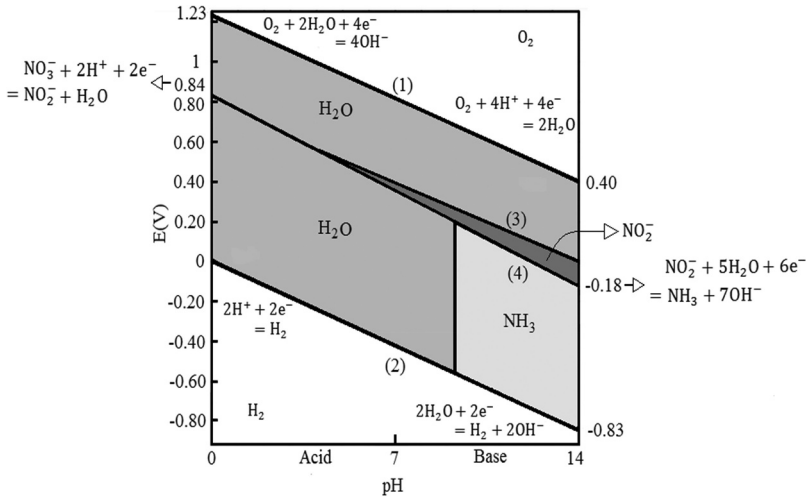

Figure 8. Pourbaix diagram of nitrogen species and in particular to show NO_2^-/NH_3 equilibrium.

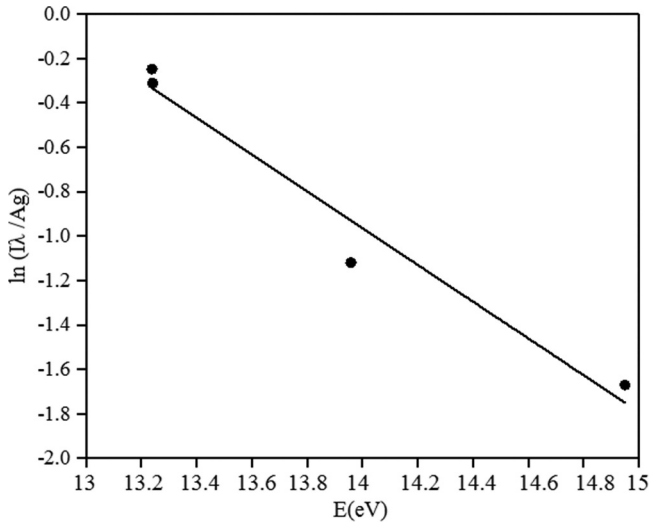

Figure 9. The Boltzmann plot of N I spectral lines used to measure plasma electron temperature at 8kv.

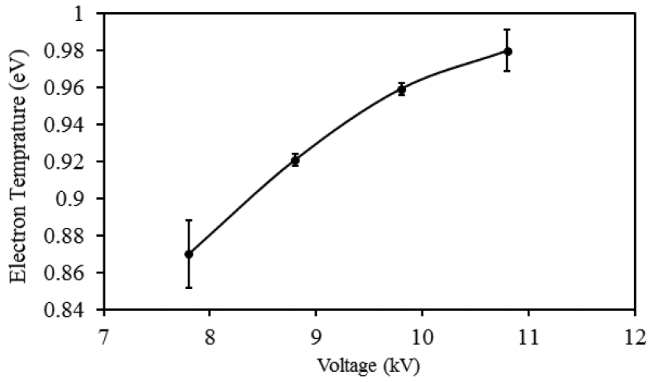

Figure 10. Temperature of resulting plasma at 8kv, 9kv, 10kv, and 11kv.

density by analyzing the full-width at half-maximum (FWHM). The FWHM of the Stark broadening relating to the electron density is defined by eq. (2) [72,73]

$$\Delta\lambda_{\text{stark}} = 4.8(\text{nm})\left(\frac{n_e}{10^{23}}\right)^{0.68116} \tag{18}$$

The Stark broadening of $H_\beta$is related to the Lorentz and the Van der Waals broadening through eq. (19) [74]

$$\Delta\lambda_{\text{stark}} = \Delta\lambda_{\text{Lorentz}} - \Delta\lambda_{\text{Vander Waals}} \tag{19}$$

So the Stark broadening is calculated using the Lorentz and the Vander Waals broadenings. The Lorentz broadening is calculated by the fitting of experimental spectra with Voigt profile (the superposition of Gauss and Lorentz broadenings). The Van der Waals broadening is because of the dipole moment induced by neutral perturber foreign gas species interacting with the electric field of the excited emitter atom, and it causes line profiles of Lorentzian shape. FWHM of the Vander Waals broadening is determined as follows [72,74]

$$\Delta\lambda_{\text{VanderWaals}} = (3.6)\left(\frac{P(\text{atm})}{T_g^{0.7}(K)}\right) \tag{20}$$

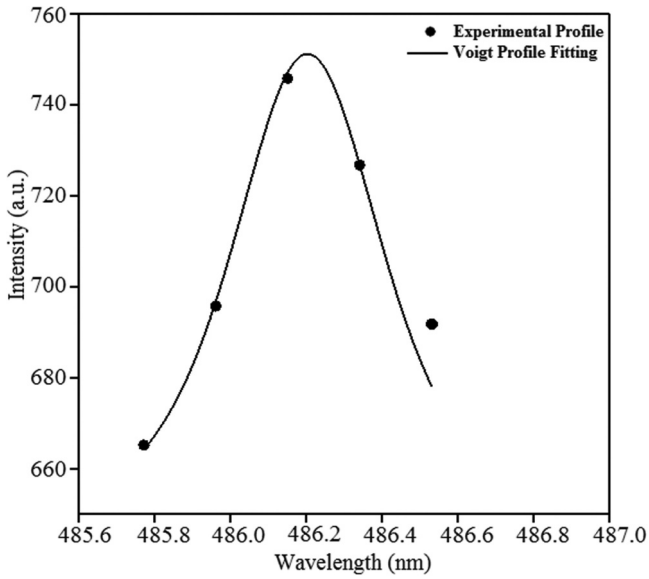

Figure 11. The typical Voigt-function fitting of the H_β experimental profile of N I spectral lines used to measure plasma density at 8kv.

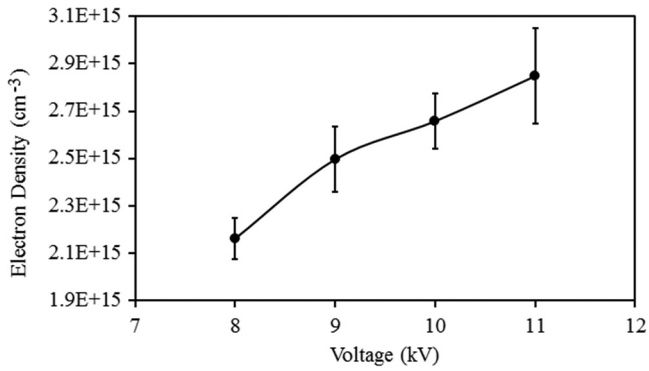

Figure 12. Density of resulting plasma at 8kv, 9kv, 10kv, and 11kv.

where T = 300Kand P = 1atm. Figure 11 presents the typical Voigt-function fitting of the H_β experimental profile at the voltage of 8kV.

Figure 12 shows density changes at voltages 8kV, 9kV, 10kV, and 11kV with values of $2.162 \times 10^{15}\text{cm}^{-3}$, $2.497 \times 10^{15}\text{cm}^{-3}$, $2.658 \times 10^{15}\text{cm}^{-3}$, and $2.848 \times 10^{15}\text{cm}^{-3}$, respectively.

Voltage–current characteristic and multiple parameters linear regression (MLR)

The voltage generated in electrolysis is the difference in electrical potential between the cathode and anode sides of the H-shaped reactor. Electrolysis has an electrical potential as a result of electron competition. According to Fig. 13, the voltage – current diagram of water classical electrolysis, the current increases with the voltage. In the first part (A), non-Faradic region, the current increases slowly with the potential. Electrolysis has not begun in this region. The Faradaic region is where the current flows through the reactor as a result of a reduction or oxidation reaction occurring at the surface of electrodes. Current and voltage at point (B) are defined as

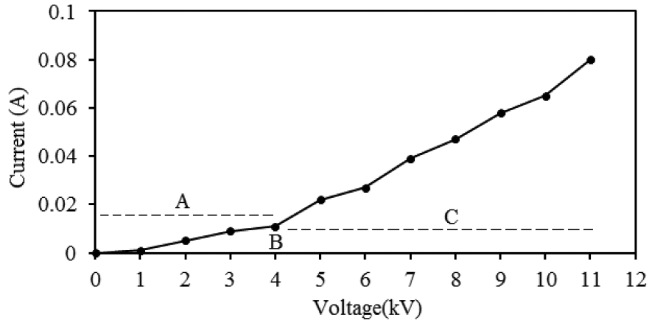

Figure 13. The I-V diagram of water classical electrolysis.

background current and dissociation potential, respectively. At potentials above point (B), Faradic region (C), the current increases substantially. The transition current occurs at (4 V, 0.011A). In practical situations, there is a small current in the electrolysis reactor at operating voltages less than the dissociation potential. The fitting results show two distinct linear trends previously reported.[75,76]

The voltage versus current plot of plasma electrolysis is shown in Fig. 14. By applying a small voltage in the region (A), ions and electrons are created by background ionization and current is established in the reactor. At this stage of the electrical discharge, known as dark discharge, not enough visible light is emitted. As the voltage rises further, the discharge reaches the corona area, region (B), where there is not enough current to break the gas. Only small unstable points of corona form around the electrode. When the voltage reaches the threshold value (breakdown voltage), 5kV, the background gas breaks, and the discharge proceeds by reducing and then increasing the voltage to the region of transmission to the glow (C). Eventually, the current and the excitation of the background gas are high enough that lead to the formation of plasma in the glow region (D). The V–I curve exhibits the transition trends as a low-pressure DC discharge.[77]

Plasma temperature is defined as the thermal kinetic energy per particle in (eV or °K). Plasma electron density refers to the concentration or count of ionized gas particles (electron) in a given volume. Multiple parameters linear regression were used to obtain impact percentage of plasma electron density(n_e), plasma electron temperature(T_e), and ammonia concentration ($c_{Ammonia}$)at voltages 8kV, 9kV, 10kV, and11kV. Multiple parameters linear regression is a statistical technique in which several descriptive variables are used to predict the outcome of a response variable. Use of (MLR) for Plasma-electrolysis, voltage(V) as the response variable, plasma electron temperature and density, and ammonia concentration as descriptive variables, eq. (21) was obtained

$$V = (1.80369)+(2.635)T_e+(4.662)n_e + (1.8991)c_{Ammonia} \quad (21)$$

Increasing voltage had a positive influence of 28.65% on plasma electron temperature, 50.70% on plasma electron density, and 20.65% on ammonia concentration under these conditions.

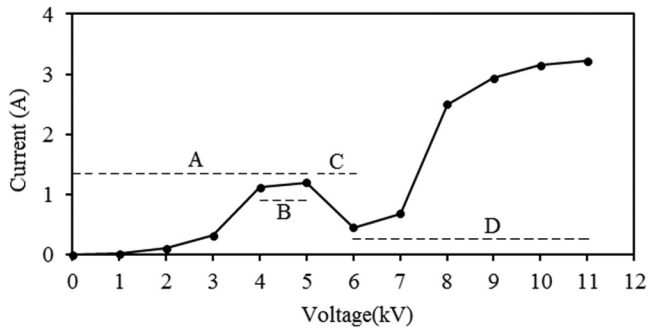

Figure 14. The I-V diagram of water plasma electrolysis.

Conclusions

In the present study, the synthesis of water-soluble ammonia by plasma electrolysis was investigated utilizing nitrogen atmospheric pressure plasma by DC discharge and the model of the Hoffman electrolysis apparatus. Then, the influence of plasma characteristics such as electron temperature and density was shown on the resultant ammonia concentration. The following conclusions were drawn from this study

(i) In plasma electrolysis, in addition to the species of the classical electrolysis, the other active species were produced. The formation of nitrogen gas plasma made by-products, nitrite, and ammonia, by chemical processes in water.
(ii) The by-products produced during plasma electrolysis were known as the cause of time differences in the concentration variations of hydrogen and hydroxide ions in comparison with classical electrolysis.
(iii) The voltage increased, the ionization rate and consequently plasma electron density enhanced which raised plasma electron temperature. High density and temperature had a constructive effect on the population involved in the reactions between plasma and the water surface. Increasing the applied voltage enhanced the electron temperature and density, followed by the concentration of water-soluble ammonia.
(iv) The impact percentages of increasing voltage on plasma electron density (50.70%), temperature (28.65%), and ammonia concentration (20.65%) were positive, respectively.

Disclosure statement

No potential conflict of interest was reported by the author(s).

References

[1] Kamo, M.; Sato, Y.; Matsumoto, S.; Setaka, N. Diamond Synthesis from Gas Phase in Microwave Plasma. *J. Cryst. Growth*. 1983, *62* (3), 642–644. DOI. DOI: 10.1016/0022-0248(83)90411-6.
[2] Saito, Y.; Matsuda, S.; Nogita, S. Synthesis of Diamond by Decomposition of Methane in Microwave Plasma. *J. Mater. Sci. Lett*. 1986, *5*(5), 565–568. DOI: 10.1007/bf01728692.
[3] Saito, Y.; Sato, K.; Tanaka, H.; Fujita, K.; Matuda, S. Diamond Synthesis from Methane-Hydrogen-Water Mixed Gas Using a Microwave Plasma. *J. Mater. Sci*. 1988, *23*(3), 842–846. DOI: 10.1007/BF01153976.

[4] Shinde, K. P.; Ranot, M.; Choi, C. J.; Kim, H. S.; Chung, K. C. Plasma-Assisted Synthesis and Study of Structural and Magnetic Properties of Fe/c Core Shell. *AIP Adv*. 2017, *7*(7), 075013. DOI: 10.1063/1.4985669.
[5] Libenská, H.; Hanuš, J.; Košutová, T.; Dopita, M.; Kylián, O.; Cieslar, M.; Choukourov, A.; Biederman, H. Plasma-Based Synthesis of Iron Carbide Nanoparticles. *Plasma Processes Polym*. 2020, *17*(11), 2000105. DOI: 10.1002/ppap.202000105.
[6] Kareem, T. A.; Kaliani, A. A. Glow Discharge Plasma Electrolysis for Nanoparticles Synthesis. *Ionics*. 2012, *18*(3), 315–327. DOI: 10.1007/s11581-011-0639-y.
[7] Vollath, D.; Sickafus, K. E. Synthesis of Nanosized Ceramic Oxide Powders by Microwave Plasma Reactions. *Nanostr. Materials*. 1992, *1*(5), 427–437. DOI: 10.1016/0965-9773(92)-90093-d.
[8] Szépvölgyi, J.; Mohai, I.; Károly, Z.; Gál, L. Synthesis of Nanosized Ceramic Powders in a Radiofrequency Thermal Plasma Reactor. *J. Eur. Ceram. Soc*. 2008, *28*(5), 895–899. DOI: 10.1016/j.jeurceramsoc.2007.09.034.
[9] Rezaei, F.; Nikiforov, A.; Morent, R.; De Geyter, N. Plasma Modification of Poly Lactic Acid Solutions to Generate High Quality Electrospun PLA Nanofibers. *Sci. Rep*. 2018, *8*(1), 2241. DOI: 10.1038/s41598-018-20714-5.
[10] Rezaei, F.; Gorbanev, Y.; Chys, M.; Nikiforov, A.; Van Hulle, S. W. H.; Cos, P.; Bogaerts, A.; De Geyter, N. Investigation of Plasma-Induced Chemistry in Organic Solutions for Enhanced Electrospun PLA Nanofibers. *Plasma Process. Polym*. 2018, *15*(6), e1700226. DOI: 10.1002/ppap.201700226.
[11] Kortshagen, U. Nonthermal Plasma Synthesis of Nanocrystals: Fundamentals, Applications, and Future Research Needs. *Plasma Chem. Plasma Process*. 2016, *36*(1), 73–84. DOI: 10.1007/s11090-015-9663-4.
[12] Kortshagen, U. R.; Sankaran, R. M.; Pereira, R. N.; Girshick, S. L.; Wu, J. J.; Aydil, E. S. Nonthermal Plasma Synthesis of Nanocrystals: Fundamental Principles, Materials, and Applications. *Chem. Rev*. 2016, *116*(18), 11061–11127. DOI: 10.1021/acs.chemrev.6b00039.
[13] Eliasson, B.; Hirth, M.; Kogelschatz, U. Ozone Synthesis from Oxygen in Dielectric Barrier Discharges. *J. Phys D: Appl Phys*. 1987, *20*(11), 1421–1437. DOI: 10.1088/0022-3727/20/11/010.
[14] Pekárek, S. Non-Thermal Plasma Ozone Generation. *Acta Polytech*. 2003, *43*(6), 47–51. DOI. DOI: 10.14311/498.
[15] Malik, M. A.; Hughes, D. Ozone Synthesis Improves by Increasing Number Density of Plasma Channels and Lower Voltage in a Nonthermal Plasma. *J. Phys D: Appl Phys*. 2016, *49*(13), 135202. DOI: 10.1088/0022-3727/49/13/135202.
[16] Patil, B. S.; Wang, Q.; Hessel, V.; Lang, J. Plasma N2-Fixation: 1900-2014. *Catal. Today*. 2015, *256*(1), 49–66. DOI: 10.1016/j.cattod.2015.05.005.
[17] Chen, H.; Yuan, D.; Wu, A.; Lin, X.; Li, X. Review of Low-Temperature Plasma Nitrogen Fixation Technology. *Waste Dispos. Sustain. Energy*. 2021, *3*(3), 201–217. DOI: 10.1007/s42768-021-00074-z.
[18] Sugiyama, K.; Akazawa, K.; Oshima, M.; Miura, H.; Matsuda, T.; Nomura, O. Ammonia Synthesis by Means of Plasma Over MgO Catalyst. *Plasma Chem. Plasma Process*. 1986, *6*(2), 179–193. DOI: 10.1007/BF00571275.
[19] Yin, K. S.; Venugopalan, M. Plasma Chemical Synthesis. I. Effect of Electrode Material on the Synthesis of Ammonia. *Plasma Chem. Plasma Process*. 1983, *3*(3), 343–350. DOI: 10.1007/BF00564632.
[20] Miura, H.; Sugiyam, K.; Oshima, M.; Kanagawa, S.; Matsuda, T.; Mitamura, T.; Nomura, O. The Formation of Ammonia in the After-Glow Region of N_2 Plasma. *Denki Kagaku*. 1988, *56*(8), 656–657. DOI: 10.5796/kogyobutsurikagaku.56.656.
[21] Uyama, H.; Matsumoto, O. Synthesis of Ammonia in High-Frequency Discharges. II. Synthesis of Ammonia in a Microwave Discharge Under Various Conditions. *Plasma Chem. Plasma Process*. 1989, *9*(3), 421–432. DOI: 10.1007/BF01083676.
[22] Nakajima, J.; Sekiguchi, H. Synthesis of Ammonia Using Microwave Discharge at Atmospheric Pressure. *Thin Solid Films*. 2008, *516*(13), 4446–4451. DOI: 10.1016/j.tsf.2007.10.053.
[23] Uyama, H.; Nakamura, T.; Tanaka, S.; Matsumoto, O. Catalytic Effect of Iron Wires on the Syntheses of Ammonia and Hydrazine in a Radio-Frequency Discharge. *Plasma Chem. Plasma Process*. 1993, *13*(1), 117–131. DOI: 10.1007/BF01447174.
[24] Bai, M.; Zhang, Z.; Bai, X.; Bai, M.; Ning, W. Plasma Synthesis of Ammonia with a Microgap Dielectric Barrier Discharge at Ambient Pressure. *IEEE Trans. Plasma. Sci*. 2003, *31*(6), 1285–1291. DOI: 10.1109/TPS.2003.818761.
[25] Bai, M.; Zhang, Z.; Bai, M.; Bai, X.; Gao, H. Synthesis of Ammonia Using CH_4/N_2 Plasmas Based on Micro-Gap Discharge Under Environmentally Friendly Condition. *Plasma Chem. Plasma Process*. 2008, *28*(4), 405–414. DOI: 10.1007/s11090-008-9132-4.
[26] Mizushima, T.; Matsumoto, K.; Sugoh, J.; Ohkita, H.; Kakuta, N. Tubular Membrane-Like Catalyst for Reactor with Dielectric-Barrier-Discharge Plasma and Its Performance in Ammonia Synthesis. *Appl Catal A-Gen*. 2004, *265*(1), 53–59. DOI: 10.1016/j.apcata.2004.01.002.
[27] Soday, F. J. Ammonia as a Petrochemical Raw Material. *Financial Anal. J*. 1951, *7*(4), 41–51. DOI. DOI: 10.2469/faj.v7.n4.41.
[28] Zumdahl, S. S. Ammonia, Encyclopedia Britannica, Oct 8, 2020. https://www.britannica.com/science/ammonia (accessed Apr 1 2022).
[29] Smil, V. Detonator of the Population Explosion. *Nature*. 1999, *400* (6743), 415. DOI: 10.1038/22672.
[30] Kang, M.; Park, E. D.; Kim, J. M.; Yie, J. E. Manganese Oxide Catalysts for Nox Reduction with NH_3 at Low Temperatures. *Appl Catal A-Gen*. 2007, *327*(2), 261–269. DOI: 10.1016/j.apcata.2007.05.024.
[31] Valera-Medinaa, A.; Xiaoa, H.; Owen-Jones, M.; David, W. I. F.; Bowen, P. J. Ammonia for Power. *Prog. Energy Combust. Sci*. 2018, *69*, 63–102. DOI: 10.1016/j.pecs.2018.07.001.
[32] Smith, C.; Hill, A. K.; Torrente-Murciano, L. Current and Future Role of Haber–Bosch Ammonia in a Carbon-Free Energy Landscape. *Energy Environ. Sci*. 2020, *13*(7), 331–344. DOI: 10.1039/C9EE02873K.
[33] Humphreys, J.; Lan, R.; Tao, S. Development and Recent Progress on Ammonia Synthesis Catalysts for Haber–Bosch Process. *Adv. Energy Sustain*. 2021, *2*(1), 2000043. DOI: 10.1002/aesr.202000043.
[34] Yun, D. S.; Joo, J. H.; Yu, J. H.; Yoon, H. C.; Kim, J. N.; Yoo, C. Y. Electrochemical Ammonia Synthesis from Steam and Nitrogen Using Proton Conducting Yttrium Doped Barium Zirconate Electrolyte with Silver, Platinum, and Lanthanum Strontium Cobalt Ferrite Electrocatalyst. *J. Power Sources*. 2015, *284*, 245–251. DOI: 10.1016/j.jpowsour.2015.03.002.
[35] Amar, I. A.; Lan, R.; Petit, C. T. G.; Tao, S. Solid-State Electrochemical Synthesis of Ammonia: A Review. *J. Solid State Electrochem*. 2011, *15*(9), 1845–1860. DOI: 10.1007/s10008-011-1376-x.
[36] Klinsrisuk, S.; Tao, S.; Irvine, J. T. S. 18 - Membrane Reactors for Ammonia Production. In *Membrane Reactors for Energy Applications and Basic Chemical Production*; Woodhead Publishing Series in Energy, 2015; pp. 543–563. doi:10.1016/B978-1-78242-223-5.00018-2
[37] Si, Q.; Yang, J.; Fan, J.; Qiao, L.; Li, S. Can Metal Intermixing Cooperatively Improve Perovskites as Redox Materials for Thermochemical Ammonia Synthesis? a Case Study on $(Sr,Y)(Ti,Ru)O_3$. *J. Phys. Chem. C*. 2021, *125*(31), 17019–17030. DOI: 10.1021/acs.jpcc.1c04096.
[38] Bartel, C. J.; Rumptz, J. R.; Weimer, A. W.; Holder, A. M.; Musgrave, C. B. High-Throughput Equilibrium Analysis of Active Materials for Solar Thermochemical Ammonia Synthesis. *ACS Appl. Mater. Interfaces*. 2019, *11*(28), 24850–24858. DOI: 10.1021/acsami.9b01242.

[39] Heidlage, M. G.; Kezar, E. A.; Snow, K. C.; Pfromm, P. H. Thermochemical Synthesis of Ammonia and Syngas from Natural Gas at Atmospheric Pressure. *Ind. Eng. Chem. Res*. 2017, *56*(47), 14014–14024. DOI: 10.1021/acs.iecr.7b03173.

[40] Penga, P.; Chen, P.; Schiappacasse, C.; Zhou, N.; Anderson, E.; Chen, D.; Liu, J.; Cheng, Y.; Hatzenbeller, R.; Addy, M., et al. A Review on the Non-Thermal Plasma-Assisted Ammonia Synthesis Technologies. *J. Clean. Prod*. 2018, *177*, 597–609. DOI: 10.1016/j.jclepro.2017.12.229.

[41] Cherkasov, N.; Ibhadon, A. O.; Fitzpatrick, P. A Review of the Existing and Alternative Methods for Greener Nitrogen Fixation. *Chem. Eng. Process. Process. Intensif*. 2015, *90*, 24–33. DOI: 10.1016/j.cep.2015.02.004.

[42] Duby, P. Electrometallurgy. *Jom*. 1977, *29*(3), 13–15. DOI. DOI: 10.1007/BF03354303.

[43] Evans, J. W. *Metal Production: Electrometallurgy*. Encyclopedia of Materials: Science and Technology, 2nd ed.; Elsevier, 2003; pp 1–12. 10.1016/B0-08-043152-6/01888-X

[44] Zhang, M.; Reddy, R. G. Ionic Liquids Electrowinning of Aluminum in Batch Mode Cells. *TMS Light Metals*. 2006, *2*, 451–455.

[45] Schlesinger, M. E.; King, M. J.; Sole, K. C.; Davenport, W. G. Chapter 17 – Electrowinning. In *Extractive Metallurgy of Copper*; 5th ed.; Elsevier, 2011; pp 349–372. DOI: 10.1016/B978-0-08-096789-9.10017-4

[46] Zhang, M.; Kamavaram, V.; Reddy, R. G. Ionic Liquid Metallurgy: Novel Electrolytes for Metals Extraction and Refining Technology. *Mining Metall Explor*. 2006, *23*(4), 177–186. DOI: 10.1007/BF03403345.

[47] Judge, W. D.; Paeng, J.; Azimi, G. Electrorefining for Direct Decarburization of Molten Iron. *Nat. Mater*. 2021. DOI: 10.1038/s41563-021-01106-z.

[48] Sakamura, Y.; Omori, T. Electrolytic Reduction and Electrorefining of Uranium to Develop Pyrochemical Reprocessing of Oxide Fuels. *Nucl. Technol*. 2010, *171*(3), 266–275. DOI. DOI: 10.13182/NT10-A10861.

[49] Giurlani, W.; Zangari, G.; Gambinossi, F.; Passaponti, M.; Salvietti, E.; Di Benedetto, F.; Caporali, S.; Innocenti, M. Electroplating for Decorative Applications: Recent Trends in Research and Development. *Coatings*. 2018, *8*(8), 260. DOI. DOI: 10.3390/coatings8080260.

[50] Lodermeyer, J.; Multerer, M.; Zistler, M.; Jordan, S.; Gores, H. J.; Kipferl, W.; Diaconu, E.; Sperl, M.; Bayreuther, G. Electroplating of Dysprosium, Electrochemical Investigations, and Study of Magnetic Properties. *J. Electrochem. Soc*. 2006, *153*(4), C242. DOI: 10.1149/1.2172548.

[51] Reece Roth, J. *Industrial Plasma Engineering*; London: IOP Publishing, 1995.

[52] Bruggeman, P. J., Frontiera, R. R., Kortshagen, U. R., Kushner, M. J., Linic, S., Schatz, G. C., Andaraarachchi, H., Exarhos, S., Jones, L. O., Mueller, C. M.; et al. Plasma-Driven Solution Electrolysis. *J. Appl. Phys*. 2021, *129*(20), 200902.

[53] Zhao, Y. M.; Patange, A.; Sun, D. W.; Tiwari, B. Plasma-Activated Water: Physicochemical Properties, Microbial Inactivation Mechanisms, Factors Influencing Antimicrobial Effectiveness, and Applications in the Food Industry. *Compr. Rev. Food Sci. Food Saf*. 2020, *19*(6), 3951–3979. DOI: 10.1111/1541-4337.12644.

[54] Petrovic, S. Industrial Electrochemical Processes. Electrochemistry Crash Course for Engineers. Springer. Cham *Springer. Cham*. 2021, 65–75. DOI: 10.1007/978-3-030-61562-8_9.

[55] Shirai, N.; Uchida, S.; Tochikubo, F. Synthesis of Metal Nanoparticles by Dual Plasma Electrolysis Using Atmospheric Dc Glow Discharge in Contact with Liquid. *Jpn. J. Appl. Phys*. 2014, *53* (4), 046202. DOI. DOI: 10.7567/JJAP.53.046202.

[56] Delgado, D.; Hefter, G.; Minakshi, M. Hydrogen Generation. Alternative Energies. In *Advanced Structured Materials*; Springer, 2013; Vol. 34, pp 141–161. DOI:10.1007/978-3-642-40680-5_7.

[57] Rumbach, P.; Bartels, D. M.; Sankaran, R. M.; Go, D. B. The Solvation of Electrons by an Atmospheric-Pressure Plasma. *Nat. Commun*. 2015, *6*(1), 7248. DOI: 10.1038/ncomms8248.

[58] Chaffin, J. H.; Bobbio, S. M. H. I.; Inyang, H. I.; Kaanagbara, L. Hydrogen Production by Plasma Electrolysis. *J. Energy Eng*. 2006, *132*(3), 104–108. DOI: 10.1061/(ASCE)0733-9402(2006)132:3(104).

[59] Li, C.; Wang, T.; Gong, J. Alternative Strategies Toward Sustainable Ammonia Synthesis. *Trans. Tianjin Univ*. 2020, *26*(2), 67–91. DOI: 10.1007/s12209-020-00243-x.

[60] Van Helden, J. H.; Wagemans, W.; Yagci, G.; Zijlmans, R. A. B.; Schram, D. C.; Engeln, R.; Lombardi, G.; Stancu, G. D.; Röpcke, J. Detailed Study of the Plasma-Activated Catalytic Generation of Ammonia in N_2-H_2 Plasmas. *J. Appl. Phys*. 2002, *101*(4), 043305. DOI: 10.1063/1.2645828.

[61] Truong, N. V.; Dung, N. Q.; Huy, N. N.; Hao, P. V.; Thanh, D. V. Ultrasonic-Assisted Cathodic Plasma Electrolysis Approach for Producing of Graphene Nanosheets. *Sonochemical Reactions, IntechOpen*. DOI. 2020, 47–60. 10.5772/intechopen.89267

[62] Ganci, F.; Baguet, T.; Aiello, G.; Cusumano, V.; Mandin, P.; Sunseri, C.; Inguanta, R. Nanostructured Ni Based Anode and Cathode for Alkaline Water Electrolyzers. *Energies*. 2019, *12*(19), 3669. DOI. DOI: 10.3390/en12193669.

[63] Lei, Q.; Wang, B.; Wang, P.; Liu, S. Hydrogen Generation with Acid/alkaline Amphoteric Water Electrolysis. *J. Energy Chem*. 2019, *38*, 162–169. DOI: 10.1016/J.JECHEM.2018.12.022.

[64] Pourbaix, M.; Burbank, J. Atlas D-Equilibres Electrochimiques. *J. Electrochem. Soc*. 1964, *111*(1), 14C. DOI: 10.1149/1.2426051.

[65] Bosko, M. L.; Rodrigues, M. A. S.; Ferreira, J. Z.; Miró, E. E.; Bernardes, A. M. Nitrate Reduction of Brines from Water Desalination Plants by Membrane Electrolysis. *J. Membr. Sci*. 2014, *451*, 276–284. DOI: 10.1016/j.memsci.2013.10.004.

[66] Kaczur, J. J. Electrochemical Reduction of Nitrate. Twelfth International Forum on Electrosynthesis in the Chemical Industry: Clean and Efficient Processing, Sheraton Sand Key, Clearwater Beach, FL, October 11-15, 1998. DOI: 10.13140/RG.2.2.10271.61602.

[67] Namihira, T.; Tsukamoto, S.; Wang, D.; Katsuki, S.; Hackam, R.; Okamoto, K.; Akiyama, H. Production of Nitric Monoxide Using Pulsed Discharges for a Medical Application. *IEEE Trans. Plasma. Sci*. 2000, *28*(1), 109–114. DOI: 10.1109/27.842877.

[68] Namihira, T.; Sakai, S.; Yamaguchi, T.; Yamamoto, K.; Yamada, C.; Kiyan, T.; Sakugawa, T.; Katsuki, S.; Akiyama, H. Electron Temperature and Electron Density of Underwater Pulsed Discharge Plasma Produced by Solid-State Pulsed-Power Generator. *IEEE Trans. Plasma. Sci*. 2007, *35*(3), 614–618. DOI: 10.1109/TPS.2007.896965.

[69] Reader, J. C.; Wiese, C. H.; Martin, W. L., and A, G. *Wavelengths and Transition Probabilities for Atoms and Atomic Ions, National Standard Reference Data Series : Part I. Wavelengths - Part II*; Washington DC: *Transition Probabilities*; National Bureau Standard, 1980.

[70] Wiese, W. L.; Fuhr, J. R., and Deters, T. M. *Atomic Transition Probabilities of Carbon, Nitrogen, and Oxygen: A Critical Data Compilation (Journal of Physical and Chemical Reference Data Monograph 7)*; Maryland: American Chemical Society/American Institute of Physics, 1996.

[71] Lumma, D. *Investigation of a Diagnostic Technique for Measuring Electron Densities via Stark Broadening on the Alcator C-Mod Tokamak*; Massachusetts Institute of Technology. M.S. Massachusetts Institute of Technology, Dept. of Physics, 1996. http://hdl.handle.net/1721.1/38371

[72] Xiao, D.; Cheng, C.; Shen, J.; Lan, Y.; Xie, H. X.; Shu, X.; Meng, Y.; Li, J.; Chu, P. K. Electron Density Measurements of Atmospheric-Pressure Non-Thermal N_2 Plasma Jet by Stark Broadening and Irradiance Intensity Methods. *Phys. Plasmas*. 2014, *21*(5), 053510. DOI: 10.1063/1.4879033.

[73] Gigososa, M. A.; González, M. Á.; Cardeñosoc, V. Computer Simulated Balmer-Alpha, -Beta and -Gamma Stark Line Profiles for Non-Equilibrium Plasmas Diagnostics. *Spectrochim. Acta B: At. Spectrosc*. 2003, *58*(8), 1489–1504. DOI: 10.1016/S0584-8547(03)00097-1.

[74] Barkhordari, A.; Ganjovi, A.; Mirzaei, I.; Falahat, A.; Rostami Ravari, M. N. A Pulsed Plasma Jet with the Various Ar/n2 Mixtures. *J. Theor. Appl. Phys*. 2017, *11*(4), 301–312. DOI: 10.1007/s40094-017-0271-y.

[75] K, O.N.O. Theoretical Concept of Hydrogen Redox Electric Power Generation. *Electr. Eng. Jpn*. 2016, *197*(4), 12–24. DOI: 10.1002/eej.22881.

[76] Shen, M.; Bennett, N.; Ding, Y.; Scott, K. A Concise Model for Evaluating Water Electrolysis. *Int. J. Hydrog. Energy*. 2011, *36*(22), 14335–14341. DOI: 10.1016/j.ijhydene.2010.12.029.

[77] Schutze, A.; Jeong, J. Y.; Babayan, S. E.; Park, J.; Selwyn, G. S.; Hicks, R. F. The Atmospheric-Pressure Plasma Jet: A Review and Comparison to Other Plasma Sources. *IEEE Trans. Plasma. Sci*. 1998, *26*(6), 1685–1694. DOI: 10.1109/27.747887.